electronics

MDPI

Article

A 5.9 GHz Channel Characterization at Railroad Crossings for Train-to-Infrastructure (T2I) Communications

Junsung Choi [1] and Seungyoung Ahn [2,*]

[1] Center for Green Transportation System, KAIST, Daejeon 34051, Republic of Korea; choijs89@kiast.ac.kr
[2] Cho Chun Shik Graduate School of Mobility, KAIST, Daejeon 34051, Republic of Korea
* Correspondence: sahn@kaist.ac.kr

Abstract: Intelligent transport systems (ITSs) rely on wireless communications that provide many services to ground and aerial vehicles. We believe that vehicular communication protocols can evolve the train communication systems into the next generation. However, we found that channel models in train track environments at the 5.9 GHz frequency band are scarcer than in vehicular environments. Therefore, we conduct channel measurements at the 5.86–5.91 GHz ITS band at various railroad crossings in the United States. This allows us to extract the channel parameters and evaluate the propagation channel characteristics. The evaluations show a certain similarity between the train track channel characteristics and the vehicular communications channel characteristics. The railroad channel with an omnidirectional antenna is similar to a suburban environment in the vehicular channel, and with a bidirectional antenna, it is similar to a highway LoS environment in the vehicular channel. However, more importantly, the population of the surrounding buildings and the size of the LoS window can highly affect the RF propagation characteristics.

Keywords: wireless channel measurements; wireless channel modeling; channel sounder; railroad crossing environment; 5.9 GHz ITS band

Citation: Choi, J.; Ahn, S. A 5.9 GHz Channel Characterization at Railroad Crossings for Train-to-Infrastructure (T2I) Communications. *Electronics* **2023**, *12*, 2400. https://doi.org/10.3390/electronics12112400

Academic Editors: Hao Jiang, Ji Wang, Fengxia Han and Liang Wu

Received: 27 April 2023
Revised: 22 May 2023
Accepted: 24 May 2023
Published: 25 May 2023

1. Introduction

Accidents between trains and vehicles at train crossings are mainly caused by a driver's lack of cognition of an oncoming train. Most of these accidents happen near railroad-grade crossings. Intelligent transportation systems (ITSs) will improve the efficiency and safety of transportation by leveraging advanced wireless communications and sensor technologies and systems. The Operation Lifesaver project adapted from vehicular ad-hoc networks (VANETs) demonstrated that an early warning system could significantly improve railroad safety by avoiding vehicle collisions [1].

The vehicular communication system is the dominant system used in VANETs and ITSs [2]. It has two different forms to provide services: vehicle-to-vehicle (V2V) and vehicle-to-infrastructure (V2I) communications. The vehicular communication system operates in the 5.9 GHz ITS band: 5.850–5.925 GHz. The authors of [3–5] introduce the proposed vehicle-to-train (V2T) early warning system and present their Dedicated Short-Ranged Communication (DSRC)-aided system performance and propagation channel measurements. The DSRC is the primary protocol used for the vehicular communication system, which can be found as IEEE 802.11p. The authors of [5] present the performance of the DSRC warning system with the performance metric of PER in the same topology as the conducted channel measurement that is presented in this paper. These papers demonstrated that DSRC technology has the potential to offer a cost-effective approach for the deployment of an early warning system to avoid train-to-vehicle collisions and other railroad accidents.

The infrastructure near crossings may act as a relay to provide sufficiently reliable warning signals. In [3–5], the early warning system architecture using infrastructure

near the crossing is presented. From the results, the wireless system using the 5.9 GHz frequency band can potentially be used for train-to-infrastructure warning applications. The communications range of the vehicular communication system is sensitive to the operating environment and significantly degrades in non-line-of-sight (NLoS) channel conditions, which are observed at many railroad crossings [6].

Prior work has reported channel statistics for vehicular environments with channel statistics that can affect intra-packet channel fluctuations for large packet sizes [7–12]. Thus, knowledge of grade crossing propagation channel environment statistics will allow for the development of flexible yet robust communication protocols that can operate even under potentially degraded conditions; therefore, a presentation about generalized statistical channel conditions can provide an expectation of a system performance that will be implemented at a train track.

The studies of the propagation channels for vehicle-related environments were performed in several previous studies. Most of the studies considered V2I or V2V [13–18]. Only a few previous studies considered Train-to-Train (T2T) [19,20] or Train-to-Infrastructure (T2I) [21] environments. Interestingly, their interested frequency bands were different: 2.4 GHz [22], 2.1–2.6 GHz [21], 5.2 GHz [19], 5.9 GHz [14–16], etc. The applications that were evaluated at 5.9 GHz were V2V or V2I. The propagation channel evaluations at the environments were expected to use T2T or T2I were not using the 5.9 GHz frequency band, which is the operating band by the vehicular communication protocol. We observed from the related research surveys that studies on channel models and the measurements for the relevant T2I at 5.9 GHz frequency band scenarios are scarce. Therefore, we conducted the 5.9 GHz T2I propagation channel measurements at real operating train crossings and analyzed the propagation channel characteristics under these scenarios.

This paper presents (1) T2I channel measurements at the 5.9 GHz frequency band and (2) the propagation channel data analyses at real operating railroad tracks in the United States. This measurement campaign can be considered a rare case of a 5.9 GHz propagation channel analysis for T2I scenarios. In the later sections, we present the channel sounder tool for evaluating channels at railroad tracks and derive the path loss, path loss exponent, Ricean K-factor, RMS delay, and the Doppler spread for five crossings and two antenna types.

The rest of the paper Is organized as follows: Section 2 provides the related works; Section 3 introduces the measurement setups, including the measurement system, sites, settings, scenarios, and the data analysis methods; Section 4 presents the results of the propagation channel characteristics evaluations; and Section 5 derives the conclusions and future work.

2. Related Work

Trains are considered as part of the intelligent transportation system and multiple applications are enabled by smart and connected vehicles in the broader sense. Regarding the safety applications using wireless protocols, reference [23] explores the antenna basis for a train crossing and derives an optimal antenna pattern for practical usage. Moreover, references [3–5] presents the DSRC, a vehicular communication system protocol that uses the 5.9 GHz frequency band, which can provide sufficient safety for T2I scenarios and the potential for using the vehicular communication system for the train-safety application. Since the vehicular communication protocol uses a 5.9 GHz frequency band, studying the 5.9 GHz frequency band for T2I scenarios can help future T2I system simulations or in the performance expectation before implementing T2I communication systems.

The propagation channel measurements are conducted in various frequency bands, [24] evaluated in the Terahertz band, [25] evaluated in the 2.6 GHz band, [19] evaluated in the 5.2 GHz band, [21] evaluated in the 2.1–2.6 GHz band, and [22] evaluated in the 2.4 GHz band. These studies considered vehicle-involved scenarios with different communication system protocols than the vehicular communication system, which uses the 5.9 GHz frequency band.

The propagation channel characteristics for the 5.9 GHz vehicular communications environment are presented in [7–10,13–17]. The authors compared the results between time- and the frequency-dependent K-factor in [7] and the RMS delay in [8]. Similarly, references [9,10] presented the delay spread in environmental scenarios, such as rural, urban, and highways for the 5.9 GHz channel. References [15,16] evaluated the V2V propagation channel with characteristics of both the RMS delay and K-factor. References [13,14,17,18] conducted measurements for V2I scenarios. Reference [13] presented the path loss exponent and the RMS delay spread for a 350 m long road. Reference [14] presented the path loss exponent, K-factor, and RMS delay spread in a 120 m long underground environment. Reference [17] presented both the Doppler shift and RMS delay spread in an expressway. Reference [18] presented only a path loss for the tunnel environment. References [10,26] used the power delay profile (PDP), which we leveraged for our data analysis.

Even though many propagation channel evaluation studies for both the V2V and V2I have been performed, only a few studies are interested in train-track environments. References [19–21,26] conducted measurements with trains or near train tracks. Reference [26] used measurements to derive the empirical models for the 5.8 GHz propagation channel and railroad environments. Reference [19] conducted measurements for the T2T scenario with 5.2 GHz frequency bands. Additionally, the authors present the tapped delay line channel models and compared them with the 802.11bd simulation data. In [20], a T2T channel sounding measurement in the 5.9 GHz frequency band was presented. Reference [21] presented channel models at railways considering T2I scenarios but the selected frequency band was 2.1–2.6 GHz.

As we observed from the previous studies, most studies evaluating the 5.9 GHz band used V2V/V2I scenarios. Moreover, the propagation channel measurements and evaluations with trains or near train tracks were not performed. The categorization of previous studies is shown in Table 1. The previous studies were more likely to have measured in different frequency bands than the 5.9 GHz band. Therefore, our 5.9 GHz T2I channel measurement is rare and more directly related to the vehicular communication system protocol, which uses the 5.9 GHz frequency band.

Table 1. Categorization of previous propagation channel evaluation studies.

Reference Index	Interested Scenario	Frequency Band
[7]	V2V	5.6 GHz
[8]	V2V	5.6 GHz
[9]	V2V	5.9 GHz
[10]	V2V/V2I	5.9 GHz
[26]	T2I	5.8 GHz
[24]	T2I	THz
[25]	T2I	2.6 GHz
[13]	V2I	5.8 GHz
[14]	V2I	5.9 GHz
[15]	V2V/V2I	5.9 GHz
[16]	V2V	5.9 GHz
[17]	V2I	5.9 GHz
[18]	V2I	5.8 GHz
[19]	T2T	5.2 GHz
[21]	T2I	2.1–2.6 GHz
[20]	T2T	5.9 GHz
[22]	V2I	2.4 GHz

3. Measurement Setup

3.1. Measurement System

The measurement campaign aims to obtain the RF propagation channel parameters at the train tracks for T2I communications. The RF propagation campaign is interested in the 5.86–5.91 GHz frequency range with a direct-sequence spread spectrum (DSSS)

channel sounder. The detailed system setups are illustrated in Figure 1a, Table 2, and more thoroughly described in [26]. The sounder utilizes a 2047 maximal-length sequence to BPSK to modulate a continuous wave carrier. The used RF bandwidth is 30.72 MHz. Both the transmitter and receiver are software radio platforms running GNU Radio and using a National Instruments B210 universal software radio peripheral. The I/Q data and GPS location data are saved every 0.5 s. The PDP generation with the recorded data in the receiver is processed in the post-process stage. The detailed data analysis method is described in Section 3.2.

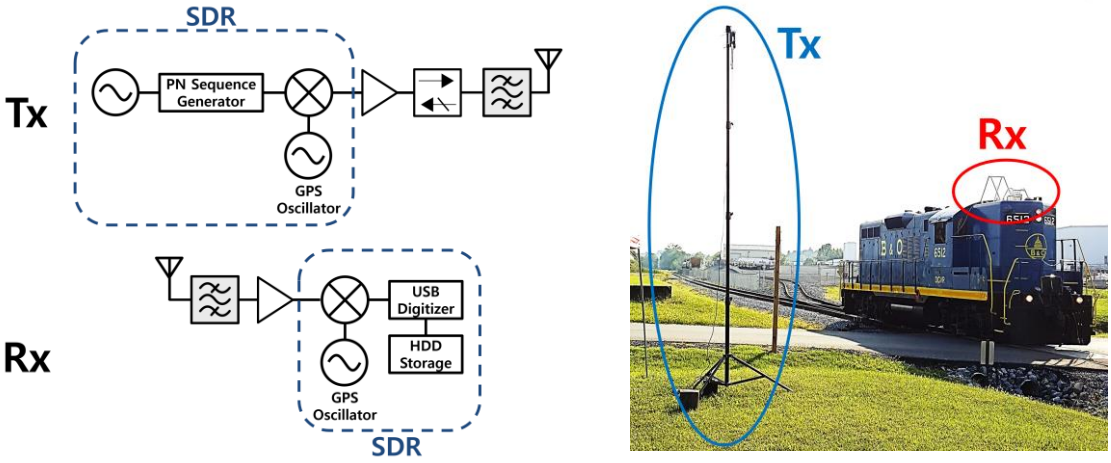

Figure 1. Channel sounder transmitter and receiver (**a**) diagram, (**b**) implementation.

Table 2. Channel sounder transmitter and receiver component specifications.

Component		Specification
Software Platform		GNU Radio
Transmitter	Amplifier	Ophir (Los Angeles, CA, USA) 5304043/50 dB Gain
	Isolator	Pasternack (Irvine, CA, USA) PE8328/2–4 GHz 20 dB Isolator
	Antenna	Mobile Mark (Itasca, IL, USA) EC012-5900 12 dBi omnidirectional antenna
	Transmission Power	10 dBm
Receiver	Amplifier	Miteq (Hauppauge, NY, USA) AFS3 0010100-20-10P-4 0.1–10 GHz 30 dB Gain
	Antenna	(1) Mobile Mark EC012-5900 12 dBi omnidirectional antenna (2) Ventev (San Antonio, TX, USA) M5000023P10006O 23 dBi bidirectional antenna
	Receive Noise Figure	<8 dB

3.2. Data Analysis Method

We used the recorded data with the channel sounder to create the PDP. The PDP contains one bin per 65 ns of delay. The I/Q data were stored in the HDD every 0.5 s. A single PDP is calculated from the correlation between the pre-defined PN sequence and one 0.5 s I/Q data. A set of PDPs composes one PDP set, which represents a single measurement. From the PDP, we evaluated the propagation channel characteristics, such as the path loss exponent, Ricean K-factor, and the Doppler spread, which were obtained from the post-processing of the recorded data.

The Ricean K-factor describes the rate between the signal powers of the line-of-sight (LoS) or dominant path and the reflected paths as Equation (1). We considered the spec-

ular power as the dominant signal power and the non-specular power as the reflected signal power in the PDP. The Ricean K-factor for a specific index can be calculated using Equation (1) for each PDP index:

$$K = \frac{\text{Specular Power}}{\text{Nonspecular Power}} \tag{1}$$

We calculated the Doppler spread (Hz), RMS delay spread (τ_{rms}), and the path loss exponent (n) by evaluating the comparison between the LoS and the multipath signals. The Doppler spread is directly obtained from the Matlabb function 'pwelch'. We set the Doppler spread as the frequency when the result of 'pwelch' was the maximum. The RMS delay spread defines how much the channel's average delay spread was captured in the specific measurement. The RMS delay spread was calculated as the square root of the second central moment of the PDP as Equation (2). The second central moment can be obtained by Equations (3) and (4):

$$\tau_{rms} = \sqrt{\overline{\tau^2} - \overline{\tau}^2} \tag{2}$$

$$\overline{\tau^2} = \frac{\sum P(\tau_i)\tau_i^2}{\sum P(\tau_i)} \tag{3}$$

$$\overline{\tau} = \frac{\sum P(\tau_i)\tau_i}{\sum P(\tau_i)} \tag{4}$$

The path loss exponent is the rate of the received signal strength decreasing with distance. The path loss exponent (n) can be calculated using Equation (5). P_t represents the transmission power; P_r represents the received power; d represents the distance between the transmitter and the receiver; and K_0 is the free-space path loss, which can be described using Equation (6):

$$n = \frac{-(P_t - P_r + 10\log_{10} K_0)}{10\log_{10} d} \tag{5}$$

$$K_0 = 20\log_{10}\frac{4\pi}{\lambda} \tag{6}$$

The post-processing was performed by Matlab script. Equations (1), (2) and (5), and the 'pwelch' function are used to calculate each propagation channel characteristic from the PDP. The procedure of the post-processing script is shown in Figure 2.

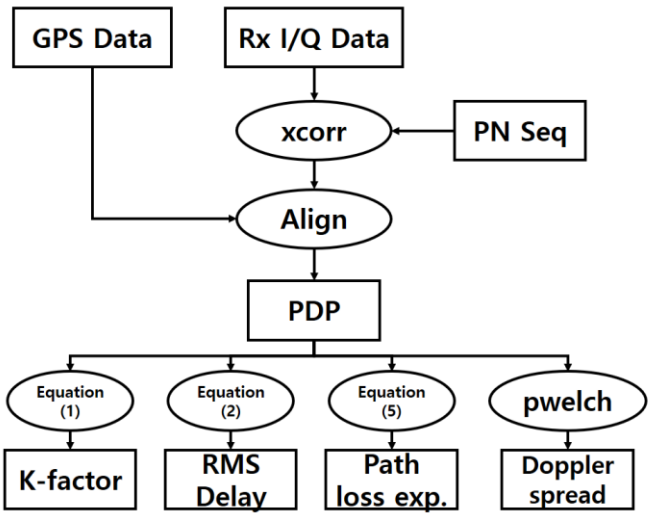

Figure 2. The procedure of post-processing Matlab script.

In order to further analysis each communication crossing environment, we compared the path loss exponents that we obtained to those suggested by the Third Generation Partnership Project (3GPP) models [27]. Specifically, we considered the following 3GPP models based on our measurement locations: Rural Macro Line-of-Sight (RMa LoS), Rural Macro Non-LoS (RMa NLoS), Urban Macro LoS (UMa LoS), Urban Macro NLoS (UMa NLoS), Suburban Macro LoS (SMa LoS), and Suburban Macro Non-LoS (SMa NLoS), [25]. Each 3GPP path loss equation for a specific scenario can be described as follow:

$$\mathrm{PL}_{\text{RMa LOS}} = 20\log_{10}\left(\frac{40\pi \mathrm{d} \mathrm{f}_\mathrm{c}}{3}\right) + 0.48\log_{10}\mathrm{d} - 0.7 + 0.0014\mathrm{d} \tag{7}$$

$$\mathrm{PL}_{\text{RMa NLOS}} = 119.53 + 38.63\left(\log_{10}\mathrm{d} - 3\right) + 20\log_{10}\mathrm{f}_\mathrm{c} \tag{8}$$

$$\mathrm{PL}_{\text{SMa LOS}} = 20\log_{10}\left(\frac{40\pi \mathrm{d} \mathrm{f}_\mathrm{c}}{3}\right) + 1.57\log_{10}\mathrm{d} - 2.31 + 0.002\mathrm{d} \tag{9}$$

$$\mathrm{PL}_{\text{SMa NLOS}} = 122.14 + 38.63\left(\log_{10}\mathrm{d} - 3\right) + 20\log_{10}\mathrm{f}_\mathrm{c} \tag{10}$$

$$\mathrm{PL}_{\text{UMa LOS}} = 22\log_{10}\mathrm{d} + 28 + 20\log_{10}\mathrm{f}_\mathrm{c} \tag{11}$$

$$\mathrm{PL}_{\text{UMa NLOS}} = 130.8 + 39.1\left(\log_{10}(\mathrm{d}) - 3\right) + 20\log_{10}(\mathrm{f}_\mathrm{c}) \tag{12}$$

The averaged propagation channel characteristics over the tested track were evaluated. For each crossing, the data were collected by three runs of the train through the tested regions. Therefore, the propagation channel characteristics averaged over the test track and three measured data sets.

3.3. Test Sites

We conducted measurements at five nearby Shenandoah Valley Railroad (SVRR) crossings, a Class 3 short-line railroad in Staunton, Virginia, U.S. As shown in Figure 3, the SVRR tracks cross a small town, and the environment near the crossings has vehicular traffic, numerous buildings, trees, and parking lots.

There are mostly open spaces (parking lots) near crossing #2. The surroundings of the other crossings have a combination of a few low-rise buildings, open spaces, and trees. Crossing #3 is placed where the train track crosses a four-lane vehicle road. Crossing #4 has the most buildings and trees in its surroundings. Crossing #5 is somewhat similar to a combination of crossings #2 and #3 due to a small LoS window, which was due to the buildings before the crossing and a mixture of open spaces and trees after the crossing. Hence, the potential shadowing and fading sources were mostly buildings, trees, and cars. Based on the surroundings, we considered crossings #1, #2, and #5 to simulate rural environments, #3 a rural-suburban environment, and #4 a suburban-urban environment.

3.4. Measurement Settings and Scenarios

The receiver was installed on the roof of the train engine, which had a height of approximately 5 m. The channel-sounder transmitter was attached to the top of a 3 m tall tripod, which was placed about 4–7 m away from the crossings. The implementation is shown in Figure 1b. The transmitter used a 12 dBi omnidirectional antenna. The receiver used a 12 dBi omnidirectional and a 23 dBi bidirectional antenna. The antenna beam patterns for an omnidirectional and a bidirectional antenna are shown in Figure 4.

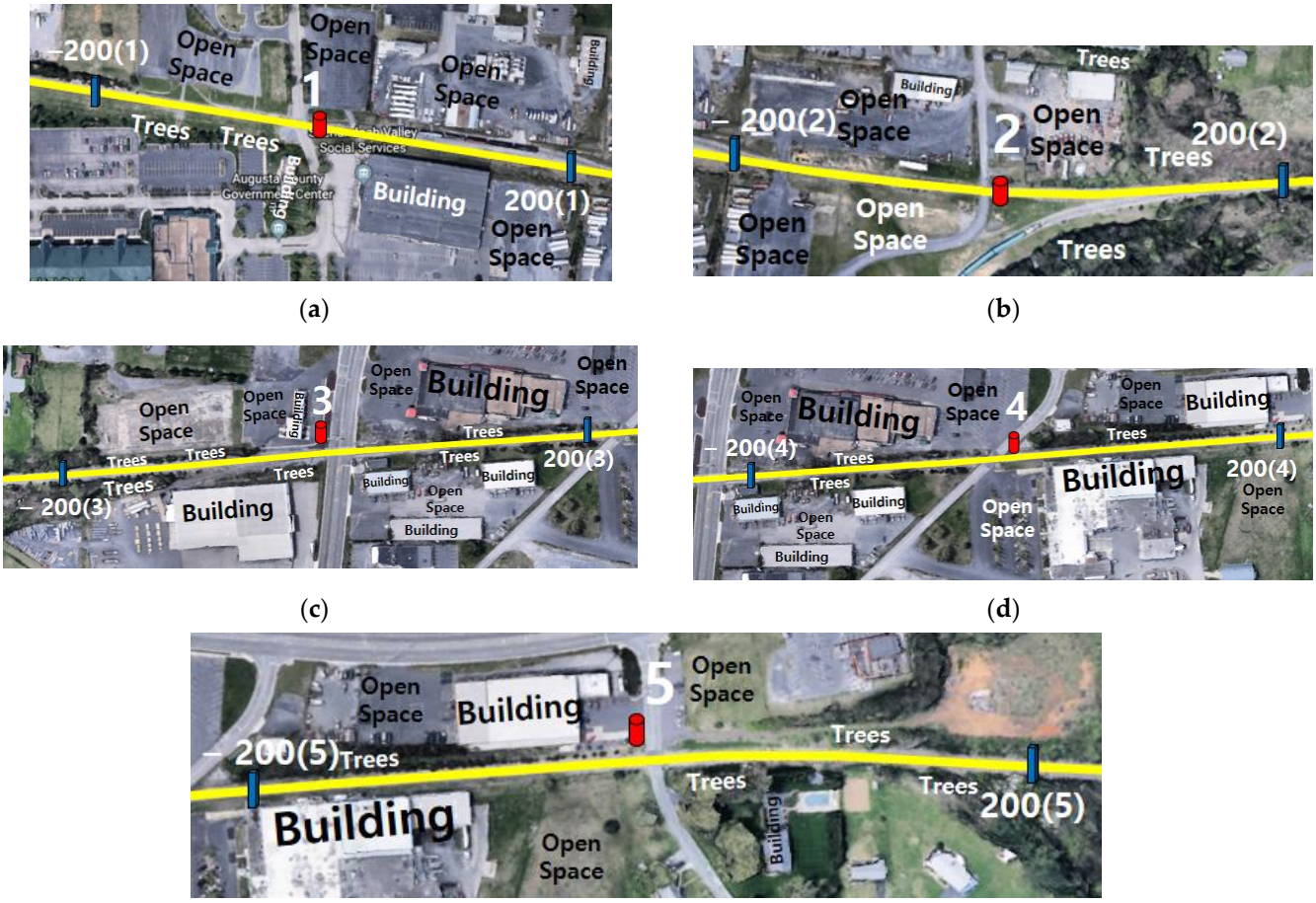

Figure 3. Test sites for five crossings of the SVRR track (**a**) crossing #1, (**b**) crossing #2, (**c**) crossing #3, (**d**) crossing #4, (**e**) crossing #5.

Prior to the measurements, we conducted an Electo-Magnetic Interference (EMI) test at 5.85–5.93 GHz along the test tracks. The purpose of the EMI test was to check the existence of any interference signals with a higher than −110 dBm signal strength. We did not observe any interference signals from the results along the test track.

The train makes three passes through the measuring regions; three sets of measured data were collected and analyzed for each crossing. The train accelerates to the desired test speed of 10 mph for each pass. The 10 mph is the maximum operating speed permitted due to the SVRR's track regulations. For all the test scenarios, the train maintained a constant speed through the tested range, which was 200 m before and after the crossing and decelerated after passing the end of the testing point, 200 m after the crossing. In Figure 3, each transmitter displacement is marked as a red bar. The testing coverage range for each crossing is marked as a blue bar and labeled as either '−200 [crossing #]' or '200 [crossing #]', which represents 200 m before and after the certain crossing #. The tested train track is colored yellow.

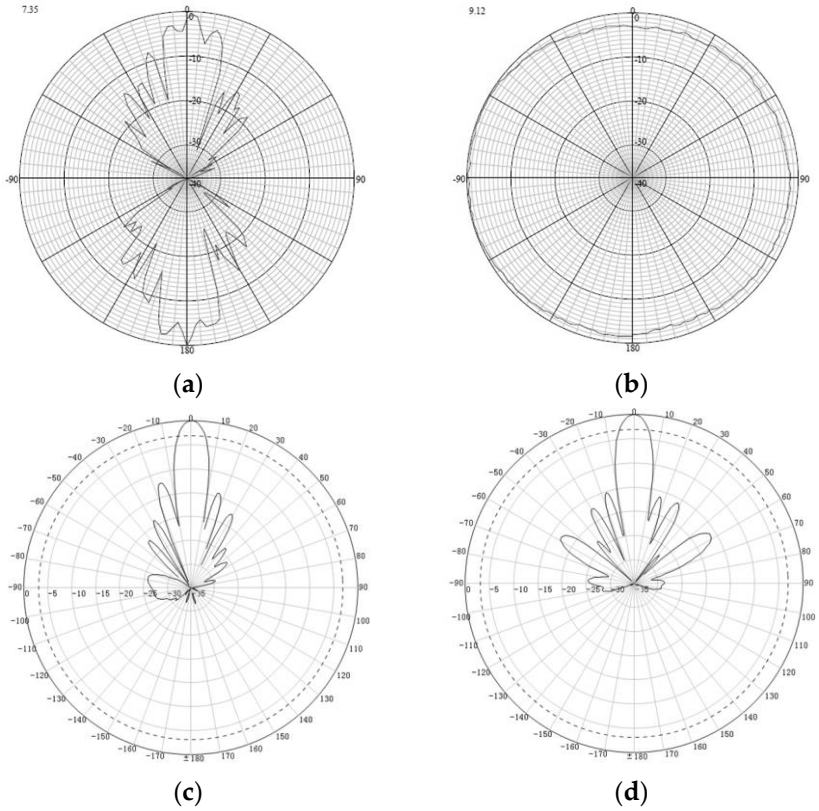

Figure 4. Antenna beam pattern (**a**) omni h-plane, (**b**) omni e-plane, (**c**) bi h-plane, (**d**) bi e-plane.

4. Result

The propagation channel characteristics for the five crossings are presented in Figures 5–9. The measured path loss values from the omnidirectional antenna with the 3GPP models are shown in Figure 5. The box plots of Figures 6–9 illustrate the distributions of the path loss exponent, Ricean K-factor, RMS delay spread, and the Doppler spread over the measurement distance of 400 m (200 m before and after each crossing) for the omnidirectional and bidirectional antenna configurations. The boxplot shows the distribution of the data including outliers, which are 1.5 IQR away from the top or bottom of the box plot and marked as '+'.

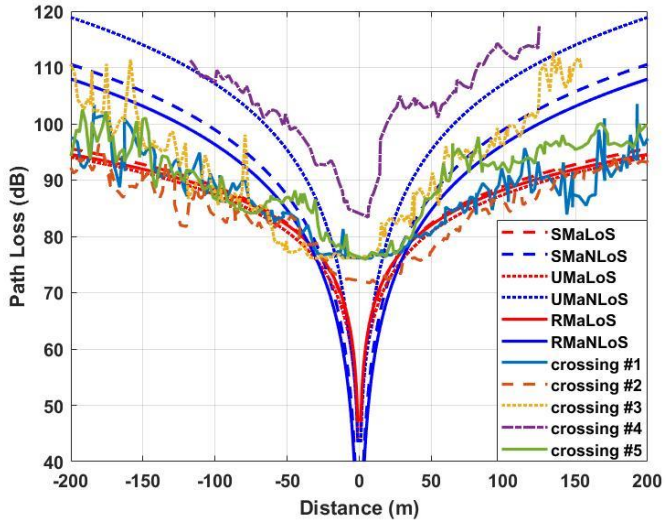

Figure 5. Path loss comparison between 3GPP path loss models and measured values for crossing #1–5 with an omnidirectional antenna.

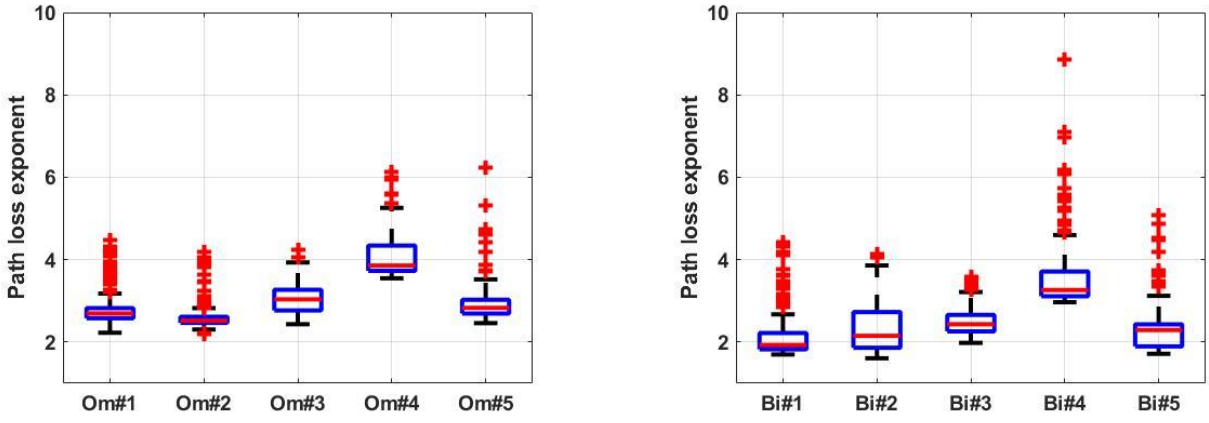

(**a**) (**b**)

Figure 6. Path loss exponents for different crossings with (**a**) omnidirectional, (**b**) bidirectional antennas.

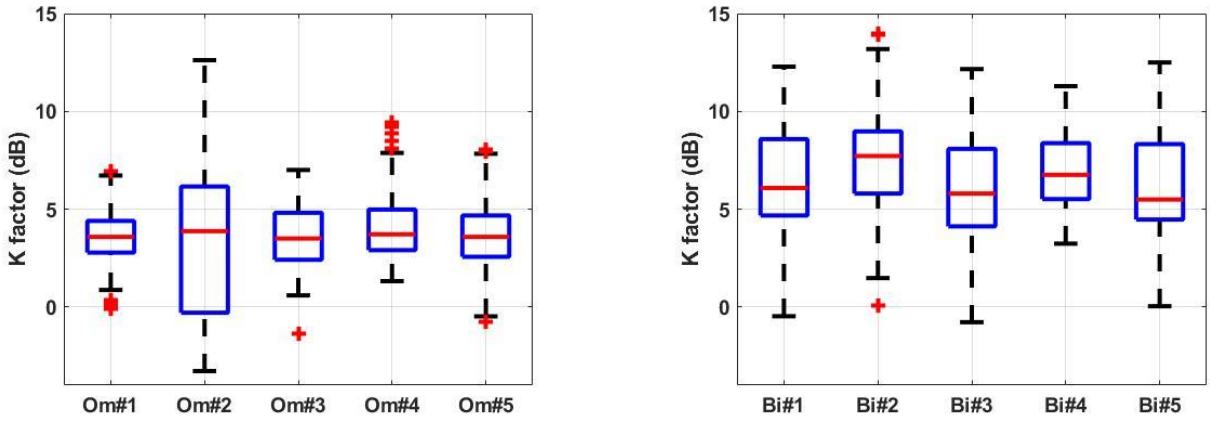

(**a**) (**b**)

Figure 7. K-factors for different crossings with (**a**) omnidirectional, (**b**) bidirectional antennas.

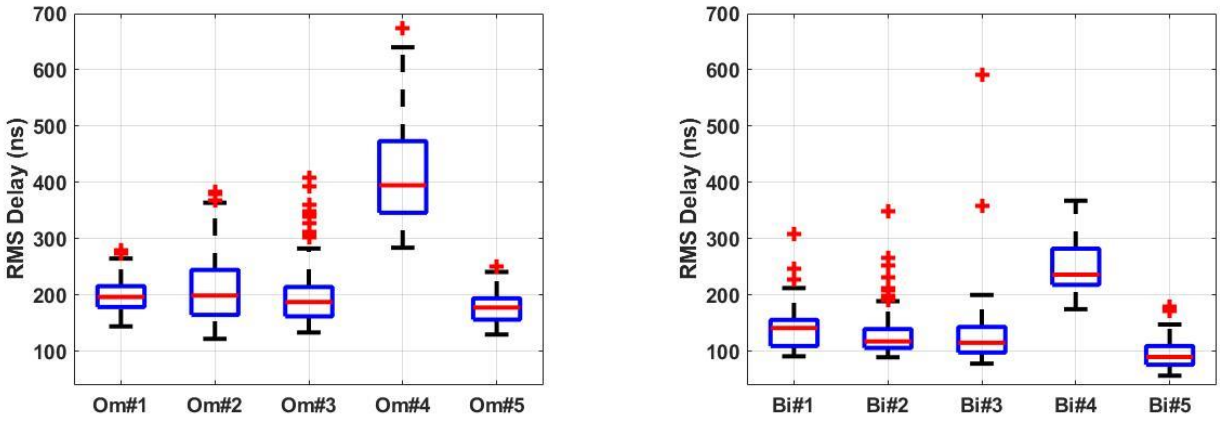

(**a**) (**b**)

Figure 8. RMS delay spreads for different crossings with (**a**) omnidirectional, (**b**) bidirectional antennas.

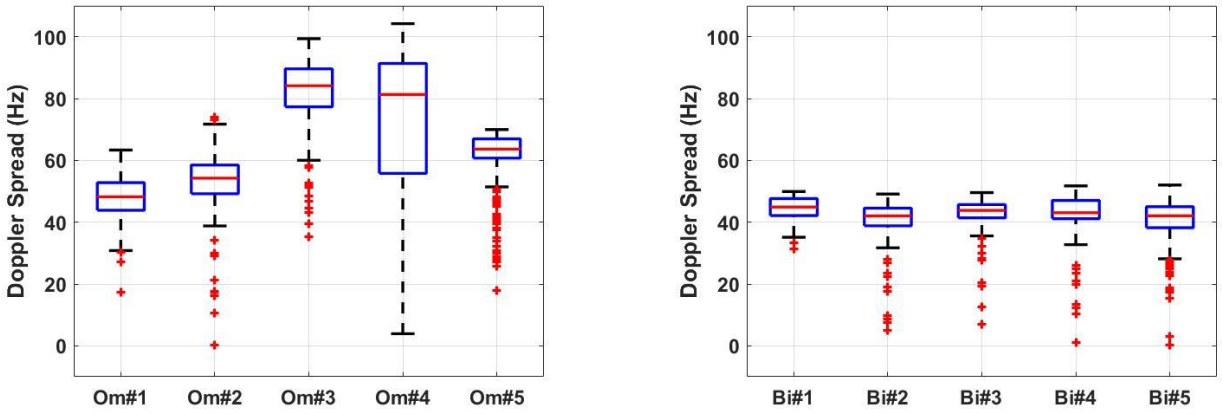

(**a**) (**b**)

Figure 9. Doppler spreads for different crossings with (**a**) omnidirectional, (**b**) bidirectional antennas.

4.1. Path Loss

By comparing the analyzed path loss and the 3GPP path loss models, crossings #1 and #2 match the model for the LoS environments. Since 3GPP path loss of LoS for urban, suburban, and rural is similar, it is hard to define a similar environment than a status of sight. Crossings #3 and #4 can be considered NLoS environments for suburban and urban, respectively. As expected, the path loss of crossing #5 is in between crossings #2 and #3. At shorter distances to the crossing, from −100 m to 0 m, the results for crossing #3, however, matched the suggested values for LoS environments. At larger distances, they match 3GPP's SMa NLoS path loss models. We assume crossing #3 can be considered a suburban environment. Interestingly, the evaluated path loss for crossing #4 is almost identical to the UMa NLoS before and worse than UMa NLoS after the crossing. Before crossing #4, the environment has combinations of small buildings, trees, and open spaces. After crossing #4, the environment has a small window of LoS and mainly has a large building near the track, which has worse conditions than before the crossing. Crossing #4 has the highest path loss and can be considered an urban-like environment.

We could expect what 3GPP path loss model to use for T2I communication from the evaluations. If the environment near the crossings is mainly trees and open spaces, the GPP RMa LoS model is preferred. If the environment has numerous buildings and trees around the crossing, the 3GPP SMa or UMa NLoS model is preferred.

4.2. Path Loss Exponent

The analyzed path loss exponents for an omnidirectional and a bidirectional antenna are presented in Figure 6. The path loss exponent determines the decay of the signal power over distance. When the path loss exponent is 2, the propagation channel behaves as free space. When the value is below 2, the channel is likely an indoor environment with strong LoS, high directivity, or where the environment acts as a waveguide. Typical outdoor terrestrial channels have path loss exponents of 2.5–4.

The average path loss exponents are between 2.60 and 2.95 for our rural-like crossings (#1, #2, and #5) and 3.05 and 4.11 for our suburban-like crossings (#3 and #4), with an exponential distribution. For the bidirectional antenna, we observe the average path loss exponent of 2.17–2.34 for the rural and 2.49–3.67 for the suburban crossings with an exponential distribution.

For all the crossings, the average path loss exponents with the bidirectional antenna are lower than with the omnidirectional antenna. This result confirms that using a bidirectional antenna can concentrate the power in the same direction as a train will move and provide more coverage range than using an omnidirectional antenna.

4.3. Ricean K-Factor

The K-factor is used to model Ricean fading, a common statistical way of representing fading with and without a strong LoS component. When no LoS component exists, K becomes 0 and behaves similar to Rayleigh fading channel characteristics. The Ricean K-factor is the ratio between the LoS and the reflected signal power.

As shown in Figure 7, the average Ricean K-factors obtained from our measurements with the omnidirectional antenna are 3.29–3.64 for our rural-like crossings (#1, #2, and #5) and 3.55–4.25 for our suburban-like crossings (#3 and #4) with a normal distribution. With the bidirectional antenna, we obtained 6.20–7.47 for our rural crossings and 5.77–6.98 for our suburban crossings, with a normal distribution. Interestingly, the average Ricean K-factors for rural-like and suburban-like crossings are not much different. Additionally, the constancy for each crossing is similar even with using different antennas. The average of Ricean K-factor when using an omnidirectional antenna is slightly lower than with a bidirectional antenna. From this behavior, we assume a communication system using a bidirectional antenna may face less of a fading effect than when using an omnidirectional antenna.

Reference [7] suggests a Ricean K-factor of 7.6 for a general LoS highway environment. The authors of [7] categorized road crossings in suburban environments with vehicular traffic (average speed of 30 km/h) and, without traffic or a smaller number of vehicles around; the evaluated K-factors were 3.7 and 4.5, respectively. Despite our initial assumptions of some crossings being in a rural area and others in suburban environments, our measurement results indicated that all five crossings with an omnidirectional antenna fall into the suburban category, and with a bidirectional antenna fall into a general LoS highway category.

4.4. RMS Delay Spread

The RMS delay spreads for an omnidirectional and a bidirectional antenna are shown in Figure 8. For the omnidirectional antenna setup, we observed the average RMS delay spread as 177.69–212.85 ns for the rural, 198.13 ns for crossing #3, and 413.98 ns for crossing #4 with an exponential distribution. For the bidirectional antenna setup, we observed the average RMS delay spread as 93.94–137.52 ns for the rural, 126.25 ns for crossing #3, and 253.04 ns for crossing #4 with an exponential distribution. From the observations, crossing #4 is more outlying than the other crossings. We assume this behavior is due to a higher population of reflecting sources near the crossing, mainly buildings. Similar to our observation for the path loss exponent for the different antenna types, the average RMS delay spreads for the bidirectional antenna were lower than for the omnidirectional antenna setup due to the concentrated beamwidth.

The omnidirectional antenna values are higher than any values reported in [8] or [9]; however, the Urban LoS reported in [10] is closer to our RMS delay spread for crossing #1, #2, #3, and #5. Our bidirectional antenna results for crossing #1, #2, #3, and #5 fall within the suburban street crossing category of [8] and the highway LoS category of [10].

4.5. Doppler Spread

The Doppler spreads for an omnidirectional and a bidirectional antenna are shown in Figure 9. The average Doppler spreads for the omnidirectional antenna were 48.00–61.22 Hz at the rural crossings and 72.57–81.00 Hz at the suburban crossings. The average Doppler spreads for the bidirectional antenna were 40.78–44.71 Hz at the rural crossings and 42.49–43.16 Hz at the suburban crossings. Interestingly, the Doppler spreads for both antenna types at rural-like crossings, crossing #1, 2, and 5, are almost constant. Additionally, more constancy was observed with the bidirectional antenna scenario. We assumed the more condensed signal power due to narrower beamwidth can minimize the noise effect. Since our measurements were performed with a 10 mph train operating speed, we could not find proper previous vehicular channel studies to compare. With a faster moving train speed, higher Doppler spread values may occur than what we present in this paper.

4.6. Summary

From the analysis of each channel parameter, we observed that crossing #4 shows scattered values, especially for the path loss exponent and the RMS delay spread with the omnidirectional antenna. Since crossing #4 has more surrounding buildings and fewer LoS window opportunities than the other crossings, we assumed that the reflecting source near the crossing and the LoS window size were dominant factors affecting the RF propagation channel.

Concerning the antenna comparison, the bidirectional antenna shows more consistent parameter values than the omnidirectional antenna because of its narrow beamwidth.

From the comparison between the presented outcomes with the results from [7–10], we examined a railroad crossing propagation channel environment similar to a suburban with an omnidirectional antenna and a highway LoS environment with a bidirectional antenna.

The mean and standard deviation of the propagation channel characteristics and the linear fitted path loss equation for the five crossings with two antenna configurations are presented in Table 3.

Table 3. Statistics of propagation channel characteristics.

	Stat	**Omni**					**Bi**				
		#1	**#2**	**#3**	**#4**	**#5**	**#1**	**#2**	**#3**	**#4**	**#5**
K-factor	μ	3.58	3.29	3.55	4.25	3.64	6.47	7.47	5.77	6.98	6.20
	σ	1.33	3.84	1.57	1.91	1.96	2.68	2.50	2.85	2.03	2.67
Path loss exponent	μ	2.78	2.61	3.05	4.11	2.95	2.17	2.34	2.50	3.67	2.33
	σ	0.38	0.31	0.36	0.60	0.49	0.59	0.59	0.34	0.96	0.57
RMS delay	μ	198.69	212.85	198.13	413.98	177.69	137.52	129.46	126.25	253.04	93.94
	σ	28.39	60.86	50.74	85.44	25.84	31.36	37.03	50.72	44.14	22.91
Doppler spread	μ	47.99	53.31	81.00	72.57	61.22	44.71	40.74	43.16	42.49	40.78
	σ	7.11	8.72	12.79	23.22	9.30	3.51	6.82	4.68	7.38	6.93
Fitted Path loss equation ($PL = a \cdot \log_{10} d + b$)	a	17.08	17.67	18.67	21.96	16.75	6.02	6.86	7.47	8.84	6.85
	b	67.11	63.05	66.51	77.77	70.50	73.78	80.00	77.13	94.52	77.33

5. Conclusions and Future Work

Collisions between trains and vehicles make up a critical portion of train accidents in the U.S. The authors of [3–5] present that vehicular communication system-aided train crossing safety warning systems can reduce the number of collisions. Additionally, an infrastructure-aided system can provide a better warning performance than a direct warning from a train to a vehicle. Since the vehicular communication system uses the 5.9 GHz spectrum and the train-related communication link is different from the usual V2V or V2I link, the measurement, evaluation of the train track propagation channel, and the comparison between previously studied vehicular channels are needed.

We conducted propagation channel measurements at several real-operating crossings of the SVRR railroad tracks. The PDP is generated from measured data, and we obtained channel characteristics from the PDP. We compared path loss with 3GPP path loss models to evaluate the path loss exponent, Ricean K-factor, RMS delay, and Doppler spread.

From the 3GPP model comparison, RMA LoS or SMa or Uma NLoS models are preferred to use depending on the environment near the crossing. The evaluated path loss exponent values with an omnidirectional antenna are 2.61–2.95 for rural-like crossings and 3.05–4.11 for suburban-like crossings and with a bidirectional antenna are 2.17–2.34 for rural-like crossings and 2.50–3.67 for suburban-like crossings. The evaluated Ricean K-factor values with an omnidirectional antenna are 3.29–3.64 dB for rural-like crossings and 3.55–4.25 dB for suburban-like crossings and with a bidirectional antenna are 6.20–7.47 dB for rural-like crossings and 5.77–6.98 dB for suburban-like crossings. The evaluated RMS delays with an omnidirectional antenna are 177.69–212.85 μs for rural-like crossings and 72.57–81.00 μs for suburban-like crossings with a bidirectional antenna are 93.94–137.52 μs

for rural-like crossings and 126.25–253.04 µs for suburban-like crossings. The evaluated Doppler spreads with an omnidirectional antenna are 47.99–61.22 Hz for rural-like crossings and 72.57–81.00 Hz for suburban-like crossings and with a bidirectional antenna are 40.74–44.71 Hz for rural-like crossings and 42.49–43.16 Hz for suburban-like crossings.

From the evaluations, we can assume that a communication system using a bidirectional will be less affected by noise from the environment near the train tracks or crossings than when using an omnidirectional antenna. Additionally, we observed that the train track and the vehicular channels have a certain similarity. The railroad channel with an omnidirectional antenna is similar to a suburban environment in the vehicular channel. Moreover, the railroad channel with a bidirectional antenna is similar to a highway LoS environment in the vehicular channel. Interestingly, the channel characteristics at crossing #4 are unique no matter what antenna is used. From the behavior, we can define that the population of the surrounding buildings and the size of the LoS window can highly affect the RF propagation characteristics.

Our experiments considered five rural-suburban combined crossings with three runs of measurements. In addition, the tested train track is two lanes. However, our data shows a little change in the fading environment along a railroad track within the range of the measuring equipment. Our measurements were conducted with a train speed of 10 mph due to regulations. However, there are faster operating train speed services provided in other countries. The propagation channels for faster-moving trains may be different than what we presented in this paper, especially in the Doppler spread. Since the train operation environment varies, more experimental data with various scenarios are needed to develop generalizable models. As wireless communication systems develop to 6G, the complexity of channel modeling will increase and require considering various scenarios [28–30]. Additionally, the frequency band will vary for 6G wireless communication systems, which will be another necessary study to be conducted [24,31,32].

Author Contributions: Methodology, J.C.; validation, J.C. and S.A.; formal analysis, J.C.; writing—original draft preparation, J.C.; writing—review and editing, J.C. and S.A. All authors have read and agreed to the published version of the manuscript.

Funding: This work was supported by Institute of Information & Communications Technology Planning & Evaluation (IITP) grant funded by the Korea government (MSIT) (No. 2022-0-00986, Development of artificial intelligence-based base station electromagnetic wave human exposure prediction algorithm).

Data Availability Statement: Data sharing is not applicable to this article.

Acknowledgments: This work was supported by Institute of Information & Communica-tions Technology Planning & Evaluation (IITP) grant funded by the Korea government (MSIT) (No. 2022-0-00986, Development of artificial intelligence-based base station electromagnetic wave human exposure prediction algorithm).

Conflicts of Interest: The authors declare no conflict of interest.

References

1. Xiang, X.; Qin, W.; Xiang, B. Research on a DSRC-Based Rear-End Collision Warning Model. *IEEE Trans. Intell. Transp. Syst.* **2014**, *15*, 1054–1065. [CrossRef]
2. Rostami, A.; Cheng, B.; Bansal, G.; Sjöberg, K.; Gruteser, M.; Kenney, J.B. Stability challenges and enhancements for vehicular channel congestion control approaches. *IEEE Trans. Intell. Transp. Syst.* **2016**, *17*, 2935–2948. [CrossRef]
3. Choi, J.; Marojevic, V.; Sharma, A.; Zewede, B.; Nealy, R.; Anderson, C.R.; Withers, J.; Dietrich, C.B. Measurement and Configuration of DSRC Radios for Vehicle-to-Train (V2T) Safety-Critical Communications. *IEEE Wirel. Commun. Lett.* **2017**, *7*, 428–431. [CrossRef]
4. Choi, J.; Marojevic, V.; Dietrich, C.B. Measurements and Analysis of DSRC for V2T Safety-Critical Communications. In Proceedings of the 2018 IEEE 88th Vehicular Technology Conference (VTC-Fall), Chicago, IL, USA, 27–30 August 2018; pp. 1–5.
5. Choi, J.; Marojevic, V.; Dietrich, C.B.; Ahn, S. DSRC-Enabled Train Safety Communication System at Unmanned Crossings. *IEEE Trans. Intell. Transp. Syst.* **2022**, *23*, 18210–18223. [CrossRef]

6. Hsu, C.W.; Liang, C.N.; Ke, L.Y.; Huang, F.Y. Verification of on-Line vehicle collision avoidance warning system using DSRC. *Int. J. Mech. Aerosp. Ind. Mechatron. Manuf. Eng.* **2009**, *3*, 808–813.
7. Bernado, L.; Zemen, T.; Tufvesson, F.; Molisch, A.F.; Mecklenbrauker, C.F. Time- and frequency-varying K-factor of non-stationary vehicular channels for safety-relevant scenarios. *IEEE Trans. Intell. Transp. Syst.* **2014**, *16*, 1007–1017. [CrossRef]
8. Bernado, L.; Zemen, T.; Tufvesson, F.; Molisch, A.F.; Mecklenbrauker, C.F. Delay and Doppler Spreads of Nonstationary Vehicular Channels for Safety-Relevant Scenarios. *IEEE Trans. Veh. Technol.* **2013**, *63*, 82–93. [CrossRef]
9. Alexander, P.; Haley, D.; Grant, A. Cooperative intelligent transport systems: 5.9-GHz field trials. *Proc. IEEE* **2011**, *99*, 1213–1235. [CrossRef]
10. Tan, I.; Tang, W.; Laberteaux, K.; Bahai, A. Measurement and analysis of wireless channel impairments in DSRC vehicular communications. In Proceedings of the 2008 IEEE International Conference on Communications, Beijing, China, 19–23 May 2008; pp. 4882–4888.
11. Cheng, L.; Henty, B.; Cooper, R.; Stancil, D.D.; Bai, F. Multi-Path Propagation Measurements for Vehicular Networks at 5.9 GHz. In Proceedings of the 2008 IEEE Wireless Communications and Networking Conference, Las Vegas, NV, USA, 31 March–3 April 2008; pp. 1239–1244.
12. Sen, I.; Matolak, D.W. Vehicle-vehicle channel models for the 5-GHz band. *IEEE Trans. Intell. Transp. Syst.* **2008**, *9*, 235–245. [CrossRef]
13. Oliveira, F.J.; Castellanos, P.V.G.; Matos, L.J.; Meza, W.D.T.; Mello, L.A.R.S. Channel Characterization on Vehicle to Infrastructure Scenarios in 5.8 GHz. In Proceedings of the 2018 IEEE MTT-S Latin America Microwave Conference (LAMC 2018), Arequipa, Peru, 12–14 December 2018; pp. 1–3.
14. Chehri, H.; Chehri, A.; Hakem, N. Empirical radio channel characterization at 5.9 GHz for vehicle-to-infrastructure communication. In Proceedings of the 2019 IEEE 90th Vehicular Technology Conference (VTC2019-Fall), Honolulu, HI, USA, 22–25 September 2019; pp. 1–6.
15. Kim, C.S.; Kim, J.S.; Hong, J.Y.; Lim, J.S.; Chong, Y.J. Propagation characteristics of urban and highway vehicle-to-everything (V2X) channels at 5.9 GHz. In Proceedings of the 2021 International Conference on Information and Communication Technology Convergence (ICTC), Jeju, Republic of Korea, 20–22 October 2021; p. 8720876.
16. Chang, F.; Chen, W.; Yu, J.; Li, C.; Li, F.; Yang, K. Vehicle-to-Vehicle Propagation Channel Performance for Overtaking Cases Based on Measurements. *IEEE Access* **2019**, *7*, 150327–150338. [CrossRef]
17. Kim, H.J.; Kim, C.S.; Lim, J.S.; Hong, J.Y.; Chong, Y.J. Vehicle-to-Infrastructure radio channel delay spread measurement in expressway environment at 5.9 GHz. In Proceedings of the 2018 International Symposium on Antennas and Propagation (ISAP), Busan, Republic of Korea, 23–26 October 2018; pp. 1–2.
18. Santos, A.; Matos, L.; Castellanos, P.; Mota, V. Channel characterization in V2I system inside a tunnel in 5.8 GHz. In Proceedings of the 2021 SBMO/IEEE MTT-S International Microwave and Optoelectronics Conference (IMOC), Fortalez, Brazil, 24–27 October 2021; pp. 1–3.
19. Bigñotte, E.M.; Unterhuber, P.; Gómez, A.A.; Sand, S.; Errasti, M.M. Measurement Based Tapped Delay Line Model for Train-to-Train Communications. *IEEE Trans. Veh. Technol.* **2022**, *72*, 4168–4181. [CrossRef]
20. Zelenbaba, S.; Mayer, L.W.; Mozo, E.; Wirth, F.; Hladik, R.; Gomez, A.A.; Bernado, L.; Schiefer, M.; Zemen, T. Characterization of Time-Variant Wireless Channels in Railway Communication Scenarios. In Proceedings of the 2019 IEEE 2nd 5G World Forum (5GWF), Dresden, Germany, 30 September–2 October 2019; pp. 536–541.
21. Berbineau, M.; Behaegel, R.; Garcia-Loygorri, J.M.; Torrego, R.; D'Errico, R.; Sabra, A.; Yan, Y.; Soler, J. Channel Models for Performance Evaluation of Wireless Systems in Railway Environments. *IEEE Access* **2021**, *9*, 45903–45918. [CrossRef]
22. Li, W.; Hu, X.; Gao, J.; Zhao, L.; Jiang, T. Measurements and Analysis of Propagation Channels in Vehicle-to-Infrastructure Scenarios. *IEEE Trans. Veh. Technol.* **2020**, *69*, 3550–3561. [CrossRef]
23. Ma, X.; Guha, S.; Choi, J.; Anderson, C.R.; Nealy, R.; Withers, J.; Reed, J.H.; Dietrich, C. Analysis of directional antenna for railroad crossing safety applications. In Proceedings of the 2017 14th IEEE Annual Consumer Communications & Networking Conference (CCNC), Las Vegas, NV, USA, 8–11 January 2017; pp. 1–6.
24. Guan, K.; Peng, B.; He, D.; Eckhardt, J.M.; Rey, S.; Ai, B.; Zhong, Z.; Kürner, T. Measurement, simulation, and characterization of Train-to-Infrastructure inside-station channel at the Terahertz band. *IEEE Trans. Terahertz Sci. Technol.* **2019**, *9*, 291–306. [CrossRef]
25. Domínguez-Bolaño, T.; Rodríguez-Piñeiro, J.; García-Naya, J.A.; Yin, X.; Castedo, L. Measurement-based characterization of Train-to-Infrastructure 2.6 GHz propagation channel in a modern subway station. *IEEE Access* **2018**, *6*, 52814–52830. [CrossRef]
26. Tedesso, T.W.; Rowe, C.; Anderson, C.R.; Dietrich, C.B. Propagation Measurements at 5.8 GHz for Railroad Intelligent Transportation Systems. In Proceedings of the 2017 IEEE Wireless Communications and Networking Conference (WCNC), San Francisco, CA, USA, 19–22 March 2017; pp. 1–6.
27. Third Generation Partnership Project, Technical Specification Group Radio Access Network. In *Evolved Universal Terrestrial Radio Access (E-UTRA)*; Further Advancements for E-UTRA Physical Layer Aspects (Release 9); European Telecommunications Standards Institute: Sophia Antipolis, France, 2010.
28. Jiang, H.; Mukherjee, M.; Zhou, J.; Lloret, J. Channel Modeling and Characteristics for 6G Wireless Communications. *IEEE Netw.* **2020**, *35*, 296–303. [CrossRef]
29. Bai, L.; Huang, Z.; Cheng, X. A Non-Stationary 6G UAV Channel Model With 3D Continuously Arbitrary Trajectory and Self-Rotation. *IEEE Trans. Wirel. Commun.* **2022**, *21*, 10592–10606. [CrossRef]

30. Jiang, H.; Xiong, B.; Zhang, H.; Basar, E. Hybrid Far- and Near-field Modeling for Reconfigurable Intelligent Surface Assisted V2V Channels: A Sub-Array Partition Based Approach. *IEEE Trans. Wireless. Commun.* **2023**. [CrossRef]
31. Serghiou, D.; Khalily, M.; Brown, T.W.C.; Tafazolli, R. Terahertz Channel Propagation Phenomena, Measurement Techniques and Modeling for 6G Wireless Communication Applications: A Survey, Open Challenges and Future Research Directions. *IEEE Commun. Surv. Tutorials* **2022**, *24*, 1957–1996. [CrossRef]
32. Hiang, H.; Xiong, B.; Zhang, H.; Basar, E. Physics-Based 3D End-to-End Modeling for Double-RIS Assisted Non-stationary UAV-to-Ground Communication Channels. *IEEE Trans. Commun.* **2023**. [CrossRef]